ELSEVIER

Microelectronics Journal 33 (2002) 153–159

Microelectronics Journal

www.elsevier.com/locate/mejo

Design and simulation of a high efficiency Rotman lens for mm-wave collision avoidance sensor

Leonard Hall[a,*], Hedley Hansen[b], Derek Abbott[a]

[a]*Centre for Biomedical Engineering and Department of Electrical and Electronic Engineering, Adelaide University, Adelaide, SA 5005, Australia*
[b]*DSTO, EWD, P.O. Box 1500, Salisbury, SA 5108, Australia*

Accepted 21 August 2001

Abstract

Multi-beam approaches using beamforming antenna array architectures have been identified as one solution for overcoming the limited fields-of-view provided by highly directional mm-wave sensors. They are also ideal front end systems for collision avoidance devices. Rotman lenses offer a compact, rugged and reliable alternative to electronically scanned antenna technologies but architectures that operate at frequencies < 20 GHz perform poorly at higher frequencies on account of greater losses and dispersion. This paper outlines the design process for providing Rotman-based lenses, examining various levels of simulation that are needed for designs that function at K and W-band frequencies. The impact of using microstrip structures is demonstrated. A key advantage of our approach is that it is compatible with monolithic fabrication, leading the way towards smart collision avoidance sensors. © 2002 Published by Elsevier Science Ltd.

Keywords: Smart antenna; Rotman lens; Beamforming; microantenna arrays

1. Introduction

Sensors operating in the mm-wave (20–100 GHz) band have better poor-weather performance than those operating at IR and visible wavelengths and provide better spatial resolution (and target discrimination) than microwave systems.

Beamforming mm-wave antennas have numerous applications including radar [1], communication [2,3] and biomedical systems [4,5], synthetic vision schemes and collision-avoidance systems [6–12]. Our goal is to develop collision avoidance systems for aerospace applications such as UAVs and nanosatelites [13]. The strategy is to implement a beamforming Rotman lens-based antenna array [14], operating at 37 GHz that can be monolithically fabricated so that it provides a low-cost testing platform of the design for a further version at 94 GHz. These frequencies are chosen because they are centres of atmospheric transmission bands, with the presence of O_2 and H_2O in the atmosphere causing peak absorption of mm-waves at 60 and 22 GHz respectively. Naturally occurring 37 and 94 GHz black-body radiation propagates through cloud, smoke, fog and other such aerosols, as seen by the attenuation curve in Fig. 1. This property makes the use of these frequencies extremely attractive for remote sensing applications.

2. Specifications of integrated design

Our approach to collision avoidance is to employ a passive mm-wave front-end with back end processing based on biologically inspired insect vision principles [7,15–22]. As this approach involves motion detection based on thresholded signals, our system requirements can be more relaxed than in full mm-wave imaging systems.

The initial design that is being considered is a 37 GHz lens for steering five beams with a 40° scan angle. This provides a simple prototype to enable rapid development of the techniques required for manufacture at low cost. In addition, a half-wavelength separation of beam-ports is achievable in this design and therefore spillover losses can be kept low.

The lens and the feed lines are to be implemented using microstrip fed by microstrip patch antenna elements. This architecture is best suited for providing a compact structure that is planar and compatible with printed and monolithic fabrication. It is estimated that an eleven element array aperture of 41 mm is achievable at 37 GHz and so is an aperture of 16 mm at 94 GHz. Apertures of these sizes are

* Corresponding author. Tel.: +61-8-8303-36296.
E-mail address: Leonard.Hall@adelaide.edu.au (L. Hall).

0026-2692/02/$ - see front matter © 2002 Published by Elsevier Science Ltd.
PII: S0026-2692(01)00114-8

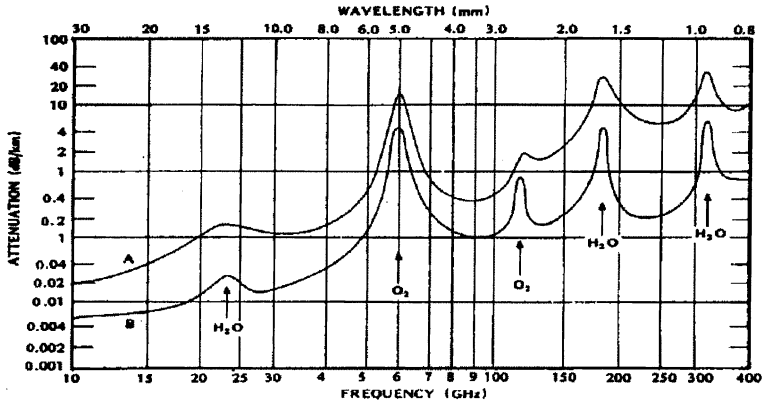

Fig. 1. The one way attenuation of electromagnetic radiation in the troposphere [23].

suitable for collision-avoidance applications and promises high gain multi-beam coverage of a 40° field-of-view.

Earlier designs employed a dipole antenna array due to the possibility of stacking 1-D arrays to form a 2-D coverage. We now pursue the patch-fed array because of its ability to conform with the skin of aircraft and cars, making the system much more compact.

3. Simulation

A Rotman lens consists of a parallel plate region (body) with beam ports and array ports distributed along opposite contours. The central beam port provides equal path lengths to each array element. An offset beam produces a path length difference and hence a phase gradient along an array, giving a steered beam.

In order to design a lens that will perform at mm-wave frequencies, three different levels of simulation are being considered. The results associated with the first two levels are reported here in detail. The third level deals not only with the simulation but also validates certain aspects of the model used.

Level one simulation involves the numerical optimisation of the Rotman geometry using ideal models [24,25]. The lens is modelled using geometric optics. No coupling between input and output ports is considered, with all ports matched and reflections and attenuation ignored.

Level two simulation addresses the non-ideal effects of the microstrip and how adopting various antenna element options affect performance [26]. Level two simulations include optimising the bandwidth performance of the lens.

Level three simulation utilises an electromagnetic simulation program such as MICRO-STRIPES [27] to calculate the *S*-matrix of various sections of the design such as ports and junctions. At this level, effects considered include the coupling between adjacent input or output ports, reflections, and unmatched ports. An electromagnetic simulation of the antenna element feeds could also be included. It is expected that only through the careful implementation of level three studies would our model be able to fully predict the performance of the lens structure.

4. Results

4.1. Level 1— ideal modelling

Scattering matrices have been used exclusively throughout the simulation, because the matrix approach allows a complete model of the lens to be developed. Initially three scattering matrices are generated, S_B accounting for the Rotman lens body, S_W for the path delays between antenna elements and associated antenna ports on the inner lens contour and S_A for the phase delays between incoming rays onto the antenna array. Combining these matrices provides the output at each port due to any given incident wave.

The design of the lens or matrix S_A is governed by the Rotman–Turner design equations that are based on the geometry of the lens and are given as follows, using the variables defined in Fig. 2:

$$y = \frac{Y}{F}$$

$$z = \frac{Z}{F}$$

$$n = \frac{N}{F}$$

$$g = \frac{G}{F}$$

$$w = \frac{W - W_o}{F}$$

$$a = \cos(\alpha)$$

$$b = \sin(\alpha)$$

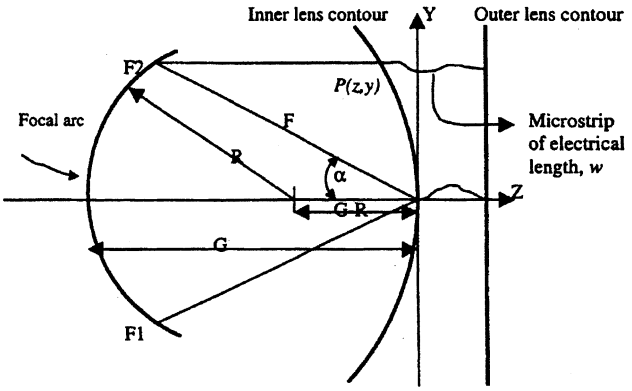

Fig. 2. Rotman lens topology [14].

$$0 = Aw^2 + Bw + C$$

$$A = 1 - \frac{(g-1)^2}{(g-a)^2} - n^2$$

$$B = -2g - n^2b^2\frac{g-1}{(g-a)^2} + 2g\frac{g-1}{g-a}$$

$$C = \frac{n^4b^4}{4(g-a)^2} + g\frac{n^4b^4}{g-a} - n^2$$

$$R = \frac{(Fa-G)^2 + F^2b^2}{2(G-Fa)}$$

where $P(Z, Y)$ is the position of the antenna ports, $P(\theta, R)$ is the position of the beam ports N is the position of each antenna in the horizontal plain and W is the added delay length between antenna and lens.

Fig. 3(a) shows the layout of the eleven antenna element, five beam port configuration under consideration where the opposite contours are clearly shown. A normalised focal length ratio of $g = 1.06$ is used with the off-axis focal point angle of 20°. Fig. 3(b) shows the desired path lengths that are needed to link antenna elements to their corresponding antenna ports. Fig. 3(c) displays the maximum phase error versus angle. For the three focal points there is no phase error at all, between these points the phase error remains $< 0.7°$. Fig. 4(c) then displays the idealized seven-beam radiation pattern. The average side lobe level for an array aperture with antenna elements spaced 0.5 wavelengths apart is -30 dB as shown in Fig. 4(a). Clearly, the amplitude and phase performance of the idealised design is acceptable.

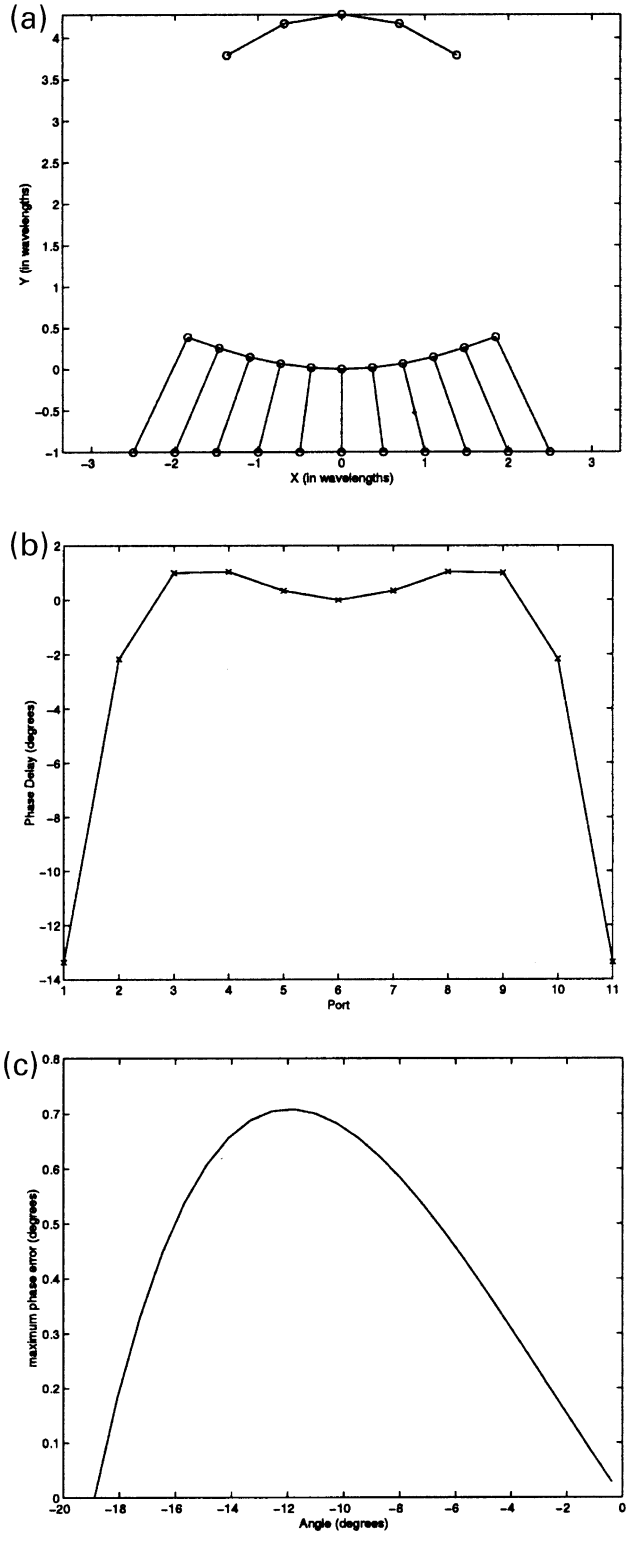

Fig. 3. Basic Rotman lens design: (a) lens layout; (b) path delay versus antenna element; (c) phase error versus beam angle.

4.2. Level 2 — non-ideal modelling

We now show the adverse affect on performance of using non-ideal antenna elements within a microstriplens structure. For this simulation, the S_A matrix is altered to account for attenuation in microstrip and a S_W matrix that uses non-ideal dipoles as antenna elements is considered.

We would expect some power to be lost in the load and we should also be able to see the effect of the antenna gain

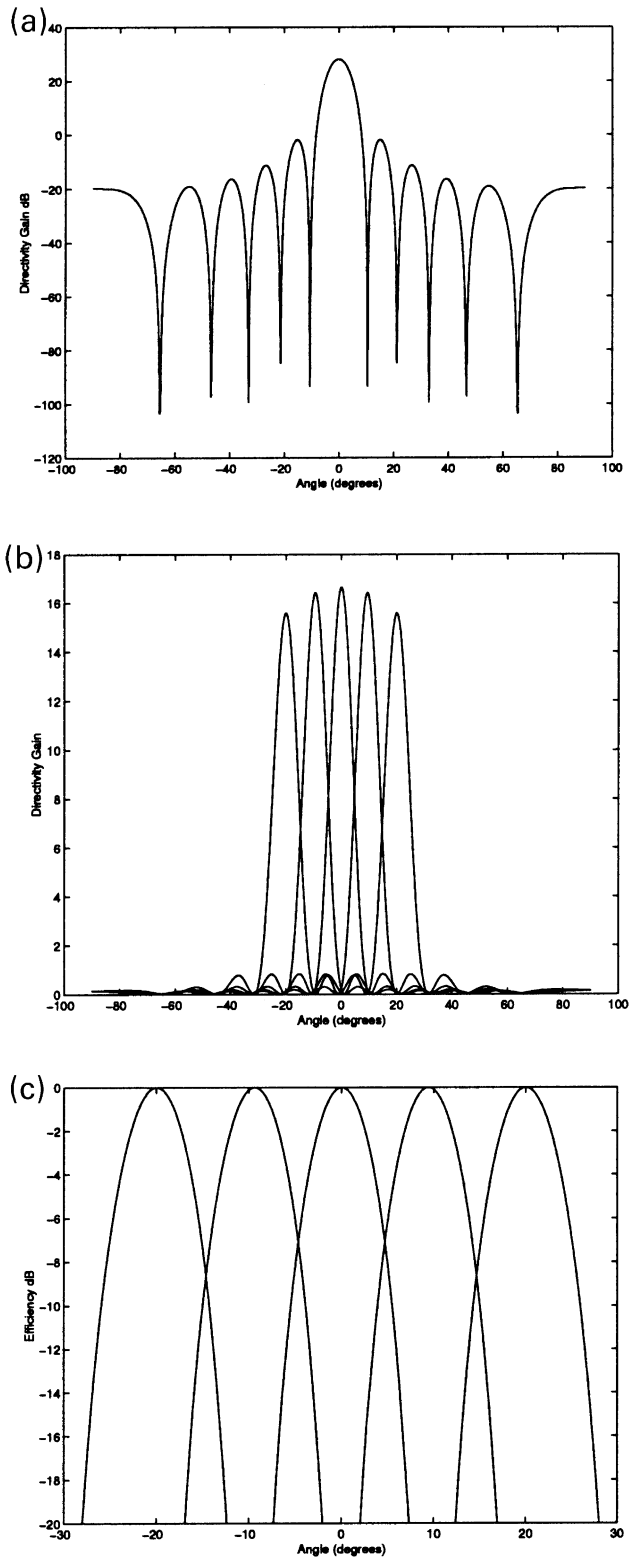

Fig. 4. Level 1 simulation results: (a) sidelobe level; (b) directivity; (c) losses.

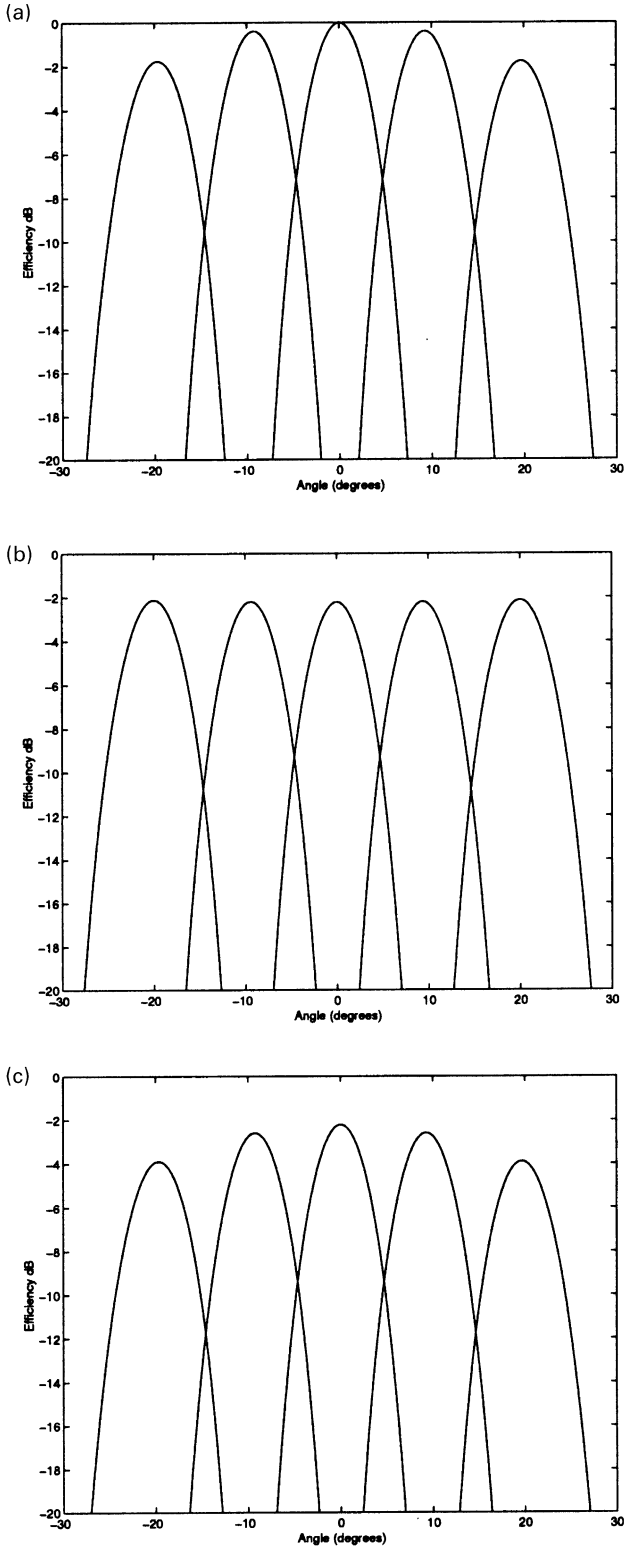

Fig. 5. Level 2 simulation results: (a) Loss due to dipole antenna. No attenuation due to microstrips or impedance mismatch; (b) Loss due to microstrip. Antenna is assumed ideal and no attenuation due to impedance mismatch; (c) Total loss due to dipole antenna and microstrips. No attenuation due to impedance mismatch.

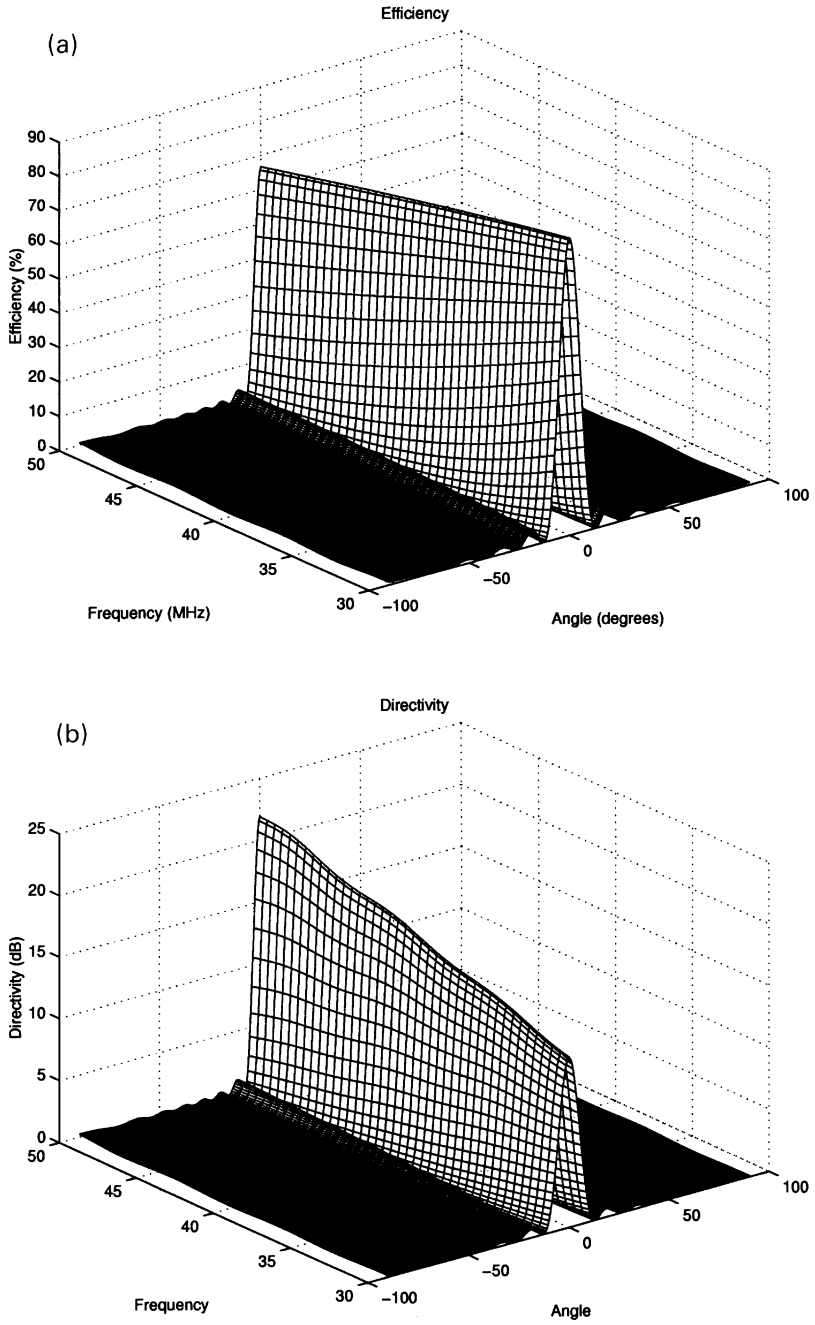

Fig. 6. Frequency dependence of Rotman lens. Isotropic frequency-independent antennas have been assumed for these graphs: (a) loss; (b) directivity.

dropping for angles other than zero degrees. Our model predicts an attenuation of 2 dB due to the microstrip line, as seen in Fig. 5(a), and the half-wave dipole will produce attenuation increasing from zero to 2 dB as we approach $\pm 20^\circ$ as shown in Fig. 5(b).

At this point all simulations have been carried out at 37 GHz. We are also interested in the performance of the lens above and below this frequency. This is achieved by varying the wavelength and repeating the process over the desired frequency range. In Fig. 6(a) we can see, as expected, that as the frequency increases the attenuation in the microstrip increases, reducing the efficiency of the system. In Fig. 6(b) we notice that the directivity of the device increases with frequency since the effective aperture is being increased — effective aperture increases due to the decrease in wavelength.

4.3. Level 3 — electromagnetic modelling

Producing a full simulation using software such as MICRO-STRIPES is not realistic due to the excessive processor time required. To combat this we have sought to produce a

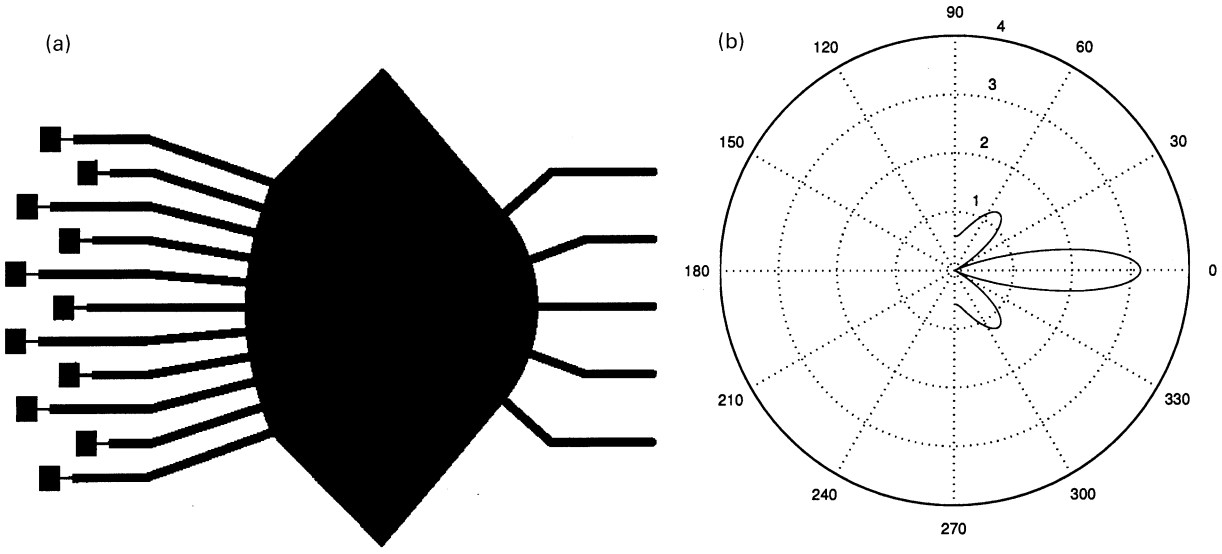

Fig. 7. Design of prototype lens: (a) Layout utilizing patch antenna; (b) Vertical directivity.

model that is initially simple and modular. By developing the modules we may easily increase the complexity and accuracy of the results.

We may also use the software to provide additional detail as required during development. We can approach the design problem in two ways. We may use the software to address the problem in our simulation or we may alter the design to minimise the effect on the system.

We use the MICRO-STRIPES [27] electromagnetic modelling software, to firstly check our assumptions such as the magnitude of losses due to microstrip lines and junctions. Secondly, using the boundary integral equation method first applied to Rotman lenses by Chan [28,29], we are able to calculate the impedance of each port along the periphery of the lens, this allows us to design separate matching networks for each of the antenna and beam ports. We are also able to calculate the coupling between all ports and in doing so calculate the scattering matrix S_B. Using this full analysis we are also able to optimise the power distribution across the antenna array to keep beam squint to a minimum.

The level 3 simulation allows us to look at the mutual coupling between antenna and the mismatch between microstrip and the body of the lens. Preliminary simulations using MICRO-STRIPES has yielded losses of around 2–5 dB between microstrip and the body of the lens, when they are directly connected. Tapered transmission lines should yield much lower losses [30,31] however, for broadband performance, much more complicated networks must be used [29]. A comprehensive simulation of these geometries will be carried out in the near future.

5. Implementation of design

We have discussed the process used to construct a model of a Rotman lens geometry. Now with the aid of this model we are able to quickly examine the effects of various design changes. Fig. 7(a) shows a design of a Rotman lens without a matching network between lens and microstrip lines. Patch antennas have a number of inherent advantages over other antenna designs because of the ease of which they are mounted and matched to the microstrip by a $\lambda/4$ impedance transformer, and their low levels of cross-coupling. The fact that patch antennas radiate perpendicularly to the surface they are mounted on, allows us to move the antenna vertically without disturbing the performance of the antenna in the horizontal plane. By fully utilising this idea we are able to keep the microstrip lines as straight as possible and avoid potential discontinuities. If the antennas are sufficiently far apart we need not include mutual coupling in our model. One important impact of this design is the reduction in the vertical beam-width. This can easily be plotted using the same ideas already discussed above. The results of these calculations are shown in Fig. 7(b), where we can clearly see the narrowing of the beam in the vertical plain and the lobes on both sides of the main beam.

6. Discussion

The modelling shows that a working integrated planar lens array for mm-wave operation in short range collision-avoidance type applications is achievable using microstrip technology. Our model predicts that a microstrip-based design will have an attenuation in the mainbeam of 2 dB as we can see in Fig. 5(c). Previous studies of similar designs have reported 2.5 dB mainbeam losses overall [20] so it is clear that minimising the microstrip paths within the lens will be a major factor in optimising performance.

The results reported are preliminary because our model

does not include any of the electromagnetic effects such as coupling between ports, reflections and the existence of propagating multiple modes. We intend to use electromagnetic simulation programs to generate the scattering matrices of geometries which include those associated with the interfacing structures into and out of the body of the Rotman lens. Ultimately, our approach should predict the sidelobe levels and mainbeam gains that are to be achieved with a fabricated device.

Acknowledgements

This research is supported by funding from the ARC, the DSTO RF Hub, and the Sir Ross and Sir Keith Smith Fund.

References

[1] N.C. Currie, C.E. Brown (Eds.), Principles and Applications of Millimeter-Wave Radar, Artech House, MA, USA, 1987.
[2] T. Ihara, T. Manabe, M. Fujita, T. Matsui, Y. Sugimoto, Research activities on millimeter-wave indoor wireless communication systems at crl, 1995 Fourth IEEE International Conference on Universal Personal Communications (1995) 197–200.
[3] T. Ihara, Y. Sugimoto, M. Fjita, Research and development project for millimeter-wave premises communication systems, Review of the Communications Research Laboratory 41 (3) (1995) 219–229.
[4] L.O. Boric, Y. Nikawa, W. Snyder, J. Lin, K. Mizuno, Novel microwave and millimeter-wave biomedical applications, 4th International Conference on Telecommunications in Modern Satellite, Cable and Broadcasting Services. TELSIKS'99 1 (1999) 186–193.
[5] O.V. Betskii, N.D. Devyatkov, V. Kislov, Low intensity millimeter waves in medicine and biology, Critical Reviews in Biomedical Engineering 28 (1-2) (2000) 247–268.
[6] A. Mohamed, A. Campbell, D. Goodfellow, D. Abbott, H. Hansen, K. Harvey, Integrated millimeter wave antenna for early warning, detection, Proceedings of SPIE Design, Characterization and Packaging for MEMS and Microelectronics (1999) 461–469.
[7] D. Abbott, A. Moini, A. Yakovleff, X.T. Nguyen, A. Blanksby, G. Kim, A. Bouzerdoum, R.E. Bogner, K. Eshraghian, A new vlsi smart sensor for colliosion avoidance inspired by insect vision, Proceedings of SPIE Intelligent Vehicle Highway Systems 2344 (1995) 105–115.
[8] D. Goodfellow, G.P. Harmer, D. Abbott, mm-Wave collision avoidance sensors: future directions, Proceedings of SPIE Sensing and Controls with Intelligent Transportation Systems 3525 (1998) 352–362.
[9] D. Abbott, A. Bouzerdoum, K. Eshraghian, Two-dimensional smart arrays for collision avoidance, Proceedings of SPIE Transportation Sensors: Collision Avoidance, Traffic Management and ITS 3207 (1998) 36–39.
[10] X. Nguyen, A. Bouzerdoum, R. Bogner, K. Eshraghian, D. Abbott, A. Moini, The stair-step tracking algorithm for velocity estimation, ANZIIS-93 (1994) 412–416.
[11] A. Yakovleff, D. Abbott, X.T. Nguyen, K. Eshraghian, Obstacle avoidance and motion-induced navigation, CAMP 95 Computer Architectures for Machine Perception Workshop (1995) 384–393.
[12] K. Chin, D. Abbott, Motion detection using colour templates, Proceedings of SPIE Design, Characterization and Packaging for MEMS and Microelectronics (1999) 314–323.
[13] D.C. Goodfellow, D. Abbott, Collision avoidance for nanosatellite clusters using millimeter-wave radiometric motion sensors, Proceedings of SPIE Electronics and Structures for MEMS 3891 (1999) 276–284.
[14] W. Rotman, R.F. Turner, Wide angle microwave lens for line source applications, IEEE Transactions of Antennas propagate AP-11 (1963) 623–632.
[15] D. Abbott, A. Moini, A. Yakovleff, X. Nguyen, R. Beare, W. Kim, A. Bouzerdoum, R.E. Bogner, K. Eshraghian, Status of recent developments in collision avoidance using motion detectors based on insect vision, Proceedings of SPIE Transportation Sensors and Controls 2902 (1997) 242–247.
[16] A. Moini, A. Bouzerdoum, A. Yakovleff, D. Abbott, O. Kim, K. Eshraghian, R.E. Bogner, An analog implementations of smart visual micro-sensor based upon insects, International Symposium on VLSI Technology, Systems, and Applications (1993) 283–287.
[17] X.T. Nguyen, K. Eshraghian, M. Moini, A. Bouzerdoum, A. Yakofleff, D. Abbott, R.E. Bogner, An implementation of smart visual micro-sensor based upon insect vision, Proceedings of 12th Aust. Micro. Conf. Micro-electronics, Meeting the Needs of Modern Technology (1993) 129–134.
[18] A. Moini, A. Bouzerdoum, K. Eshraghian, A. Yakovleff, X.T. Nguyen, A. Blanksby, R. Beare, D. Abbott, R.E. Bogner, An insect vision-based motion detection chip, IEEE JSSC 32 (1997) 279–284.
[19] D. Abbott, A. Yakovleff, A. Moini, X.T. Nguyen, A. Blanksby, R. Beare, A.S. Beaumont, G. Kim, A. Bouzerdoum, R.E. Bogner, K. Eshraghain, Biologically inspired obstacle avoidance-a technology independent paradigm, Proceedings of SPIE Mobile Robots X 2591 (1995) 2–12.
[20] D. Abbott, A. Parfitt, Collision avoidance device using passive millimetre-wave array based on insect vision, IREE 14th Australian Microelectronics Conference (Micro'97) (1997) 201–204.
[21] D. Abbott, A.J. Parfitt, Extension of the insect-vision paradigm to millimeter waves, Proceedings of SPIE Transporation Sensors 3207 (1998) 103–106.
[22] D. Abbott, A. Bouzerdoum, K. Eshraghian, Future directions for motion detection based on the parallel computational intelligence of insects, Proceedings of 23rd Euromicro Conference New Frontiers of Information Technology Short Contributions (1997) 244–249.
[23] J. Pressner, The influence of the atmosphere on passive radiometric measurements, Millimeter and Submilimeter Wave Propagation and Circuits (1979) 48/1-14.
[24] R.C. Hansen, Design trades for Rotman lenses, IEEE Transactions of Antennas Propagate 39 (1991).
[25] A.F. Peterson, E.O. Rausch, Scattering matrix intergral equation analysis for the design of a waveguide Rotman lens, IEEE Transactions of Antennas Propagate 47 (1999) 870–878.
[26] A. Balanis, Microwave Engineering, Harper and Row, New York, 1982.
[27] Kimberly Communications Consultants Ltd., MICRO-STRIPES, 2.0, 1999.
[28] K.K. Chan, Field analysis of planar bootlace lens feeds, International Conference on Radar 1 (1989) 273–278.
[29] K.K. Chan, Planar waveguide model of Rotman lens, 1989 IEEE AP-S International Symposium 2 (1989) 651–654.
[30] M. Michaelides, Microstrip transmission lines: impedance matching, coupling and filtering, Mullard Technical Communications (1972) 170–176.
[31] L. Musa, M.S. Smith, Microstrip port design and sidewall absorption for printed Rotman lenses, IEE Proceedings (Microwaves, Antennas and Propagation) 136 (1989) 53–58.